Contents lists available at *Dergipark*

Journal of Scientific Reports-A

journal homepage: *https://dergipark.org.tr/tr/pub/jsr-a*

E-ISSN: 2687-6167 ***Number 57, June 2024***

RESEARCH ARTICLE

Receive Date: 05.01.2024 *Accepted Date: 15.04.2024*

Non-linear behavior of functionally graded elastoplastic beam under torsion

Murat Karaca[a], Bahadır Alyavuz[b,*]

[a]*Gazi University, Graduate School of Natural and Applied Sciences, Ankara, Türkiye, ORCID: 0009-0009-6465-1818*
[b] *Gazi University, Faculty of Engineering, Department of Civil Engineering, Ankara, Türkiye, ORCID: 0000-0003-4643-4368*

Abstract

The torsional behavior of beams graded in one and two directions under large displacements and angular deformations was analyzed using the power law and sinusoidal functions. Functionally graded material is elastoplastic, consisting of ceramic and metal. A nonlinear finite element method with isoparametric hexahedral elements was used. The finite element formulation was developed by using the updated Lagrangian formulation based on the virtual displacement principle. An iterative solution using Newton-Raphson and updated Newton-Raphson methods was used to solve the nonlinear equation system. The propagation of the plastic region was calculated based on the flow theory of plasticity. Elastoplastic behavior and effective material properties were determined according to the TTO model. Numerical investigations have shown that functionally graded beams behave quite differently from homogeneous beams under torsion. Yielding of the material starts at the outer boundaries of the section of the homogeneous beams, and the plastic region propagates symmetrically. On the other hand, yielding and propagation of plastic regions tend to shift to regions with more ceramic volume with higher effective Young modulus in functionally graded beams. Beams graded in the axial direction have a non-linear variation of rotation angle along the axial direction, unlike beams graded in section and pure metal beams. The amount of non-linearity increases with increasing volume of the ceramic material, which has higher torsional stiffness. Unlike homogeneous beams, the largest shear stresses can occur within the section rather than at the outer boundaries of the section. In beams graded from ceramic to metal using the power law, the section moves along the transverse direction in addition to the rotation. This transverse displacement occurs in the grading direction, and its magnitude is about 3% of the thickness at 12.5° rotation angle. Also, the shear stresses are not zero in the section's midpoint. The effects of material distribution on displacements, stresses, and plastic region propagation were examined, and essential points were reported.

Keywords: Functionally graded material, torsion, hexahedral finite element.

* Corresponding author.
E-mail address: balyavuz@gazi.edu.tr

1. Introduction

Functionally graded material (FGM) was proposed by Japanese material scientists to prepare thermal barrier materials in 1984 [1]. Unlike layer-by-layer designs, a functionally graded single material structure emerges in FGM.

The use of FGMs has made it possible to eliminate apparent boundaries between layers of multilayer composites through functions called grading rules. One of these rules, the power law model, was presented at an early FGM symposium in 1990 [2]. This model is often preferred because of its wide range of material distribution. It is possible to create continuously varying material using different values of power law index [3, 4]. In addition to the power law, other functions such as exponential and sinusoidal are also used. Boggarapu et al. [5] have included the most commonly used functions in their review. Simply, these rules yield the volume fractions of the constituent materials at any point in the structure.

The effective material properties of FGM are determined through the homogenization schemes. Initial studies aimed to determine material properties up to their linear limits. A rough approach that directly relates the effective material properties to the volume fraction of materials is the scheme known as the Voigt model or the rule of mixtures. Hill [6] proposed the self-consistent scheme for materials with similar volume fractions, in which the constituents cannot be separated into the main phase and inclusion phase. Mori and Tanaka [7] later presented the Mori-Tanaka scheme for composition, in which the material microstructure can be described by the main phase and a minor inclusion phase. Since the variation of the microstructure along the grading axis limits the use of these conventional homogenization schemes, different approaches have been developed. Gasik and Lilius [8] proposed the LRVE scheme, a more comprehensive approach for FGMs. Reiter and Dvorak [9] used an approach based on combining Mori-Tanaka and self-consistent schemes. Determination of elastoplastic effective properties of non-homogeneous materials is more complicated due to additional parameters. In order to define the effective properties of elastoplastic materials in metal alloys, the scheme called TTO (Tamura-Tomota-Ozawa) model or the rule of improved mixtures, was proposed by Tamura et al. [10]. This scheme was used by Williams et al. [11] for ceramic-metal FGMs. It is based on determining effective stress and strain using the volume fractions of materials. It has been used to determine effective material properties outside the elastic limit for ceramic-metal FGMs with low ceramic volume fraction, and it is well accepted in the literature [12,13,14].

Initial studies on the torsional behavior of FGM were conducted under uniform torsion and without exceeding linear limits. Rooney and Ferrari [15] presented the analytical solution of the torsional behavior of linear elastic functionally graded (FG) bars graded in the section plane. Horgan and Chan [16] analyzed FG linear elastic bars graded in the section plane under torsion by generalizing the classic approach to inhomogeneous material. Unlike homogeneous materials, they showed that maximum shear stresses may not occur at the section boundaries. Horgan [17] later developed an analytical solution for non-isotropic FG rods. Batra [18] presented an analytical solution for a linear elastic circular cylindrical rod graded in the axial direction. Anita [19] formulated the torsional behavior of FG bars using a meshless method. Hematiyan and Estakhrian [20] presented analytical solutions for FG open section members. Nguyen et al. [21] presented analytical modeling for thin-walled FG beams. Ecsedi and Baksa [22] presented an analytical solution for the torsion of non-isotropic circular FG cylinders. Nie et al. [23] gave analytical solutions for conical cylinders graded in two directions. Akinlabi et al. [24] formulated the torsion of FG bar with a triangular cross-section. Ecsedi [25] gave the analytical solution of FG bars with elliptical cross-sections under non-uniform torsion. Tsiatas and Babouskos [26] examined the plastic region distribution under the torsional behavior of elastoplastic beams with rectangular and triangular cross-sections using the boundary element method based on the Analog Equation Method. They also included an FG beam with a rectangular cross-section in their study. Aminbaghai et al. [27] performed non-uniform torsion analyses of functionally graded I and box section beams using the power law model in the axial direction. They developed a beam element for the finite element analysis. Singh et al. [28] examined the torsional behavior of beams of various cross-sections with two homogeneous material layers in the height direction and a functionally graded transition zone between them. Chen et al. [29] proposed a

one-dimensional beam model based on the hierarchical Legendre expansion, and they examined the non-uniform torsional behavior of FG beams with various cross-sections and demonstrated the reliability of their proposed model. Mahmoodi and Malekzadeh [30] gave the analytical solutions of cracks and cavities in a rectangular cross-section bar coated by a functionally graded layer under Saint-Venant torsion. They showed FG coating layer can significantly improve the torsional behavior of isotropic bars weakened by cracks and cavities. Ecdesi and Baksa [31] gave the analytical solution for radially functionally graded orthotropic piezoelectric hollow circular cylinder under Saint-Venant torsion. They investigated the dependence of mechanical and electric fields from the power index of the radial inhomogeneity. There are also studies examining the buckling behavior of FGMs under torsional load [32,33,34].

The objective of this study is to investigate the torsional behavior and plastic region propagation of elastoplastic FG beams under large displacements and angular deformations using hexahedral finite elements. Additionally, the study aims to analyze the shear stress distribution and axial displacement distribution of elastoplastic FG beams graded according to different functions and directions.

2. Functionally graded beam

Functionally graded materials are defined by functions that eliminate material boundaries on a macro scale. In this study, the torsional behavior of beams graded using the power law and sinusoidal functions was examined. In this direction, a ceramic-metal functional graded beam was considered. The geometric properties of the beam are shown in Fig. 1. The boundary conditions are applied as a torsional loading at the $x_1=0$ and a fully clamped end at the $x_1=l$. Material grading, which differ depending on the selected function and direction, are shown in Fig. 2.

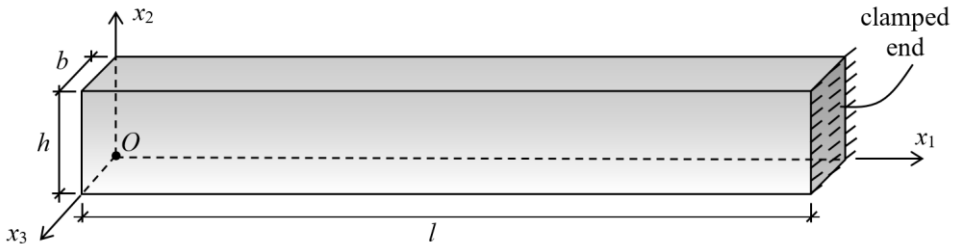

Fig. 1. Functionally graded beam.

2.1. HP-beam material grading

The beam graded using the power law along the beam height is expressed as HP-beam. The cross-section of such a beam is shown in Fig. 3a. This beam has ceramic material on the top surface and metal on the bottom. The ceramic material volume fraction and the corresponding metal material volume fraction are given in Eq. 1, and Eq.2 respectively.

$$V_c(x_2) = \left(\frac{x_2}{h}\right)^n \tag{1}$$

$$V_m(x_2) = 1 - V_c(x_2) \tag{2}$$

Positive-definite n is the parameter that determines the material distribution. V_c refers to the ceramic volume fraction and V_m refers to the metal volume fraction. If n=1, the amount of ceramic and metal materials used in the

beam are equal. The variation of ceramic volume fraction with the beam height for different *n* values is shown in Fig. 2a.

2.2. LP-beam material grading

The beam graded using the power law along the beam length is expressed as LP-beam, and it is shown in Fig. 3b. The end of the beam, where the torsional load is applied, is metal. The fully clamped end of the beam is ceramic. Ceramic volume fraction according to the power law can be calculated using Eq. 3.

$$V_c(x_1) = \left(\frac{x_1}{l}\right)^n \tag{3}$$

The variation of ceramic volume fraction along the beam for different *n* values is shown in Fig. 2a.

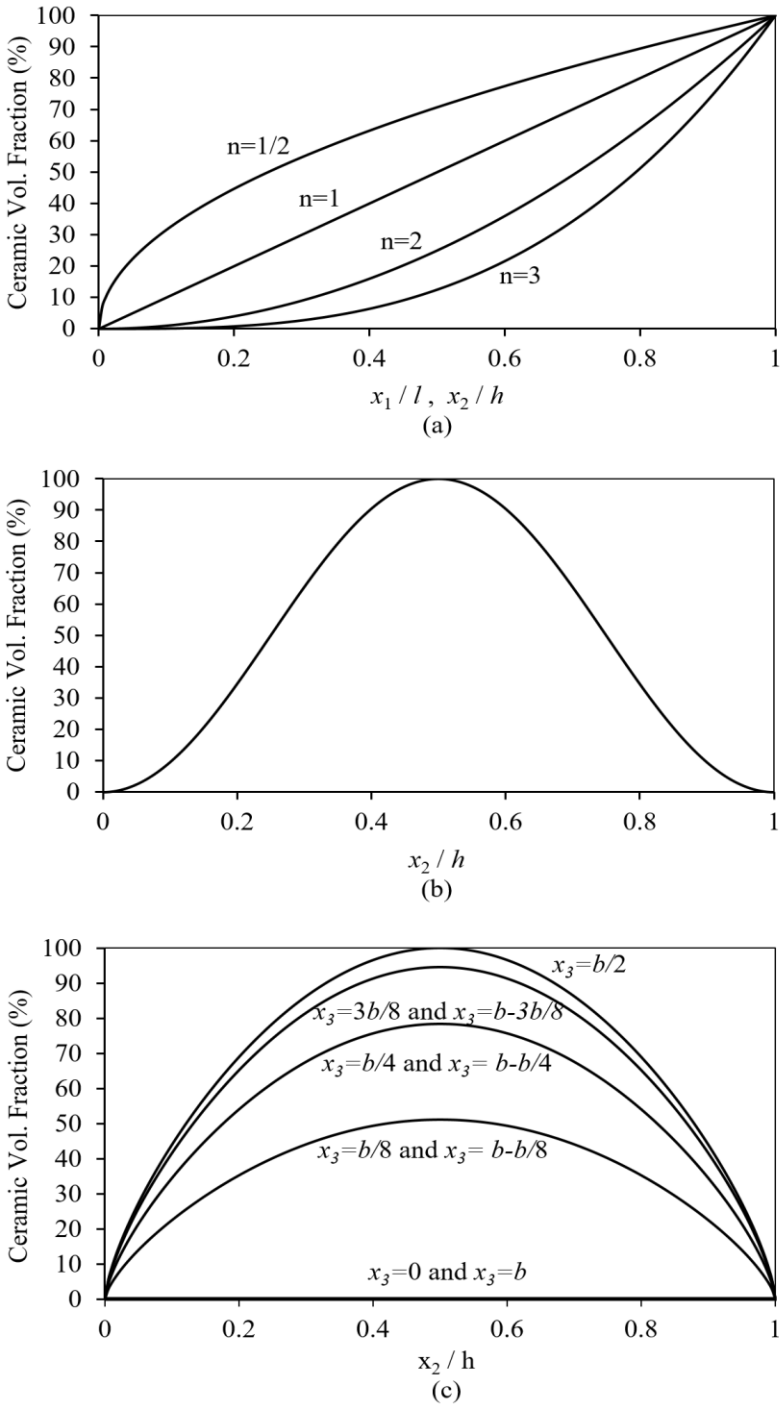

Fig. 2. The variation of ceramic volume fraction (a) HP-beam and LP- beam; (b) HS-beam; (c) HBS-beam.

2.3. HS-beam material grading

A sinusoidal grading function was used for the beam shown in Fig. 3c, with metal top and bottom surfaces. The same amount of ceramic and metal materials are used in the beam. The variation of ceramic volume fraction with the beam height is shown in Fig. 2b. Ceramic volume fraction according to the power law can be calculated using Eq. 4.

$$V_c(x_2) = \left(sin\left(\frac{\pi(2x_2-h)}{2h} + \frac{\pi}{2}\right)\right)^2 \tag{4}$$

2.4. HBS-beam material grading

Fig. 3d shows a beam graded in two directions, i.e., height and width. The metal material was used on the outer edges, and the ceramic was in the mid-region of the section. The sinusoidal function given in Eq. 5 was used as a grading function. The variation of ceramic volume fraction with beam height for specific x_3 values in the section is shown in Fig. 2c.

$$V_c(x_2, x_3) = \left(sin\left(\frac{\pi(2x_2-h)}{2h} + \frac{\pi}{2}\right) sin\left(\frac{\pi(2x_3-b)}{2b} + \frac{\pi}{2}\right)\right)^{0.7} \tag{5}$$

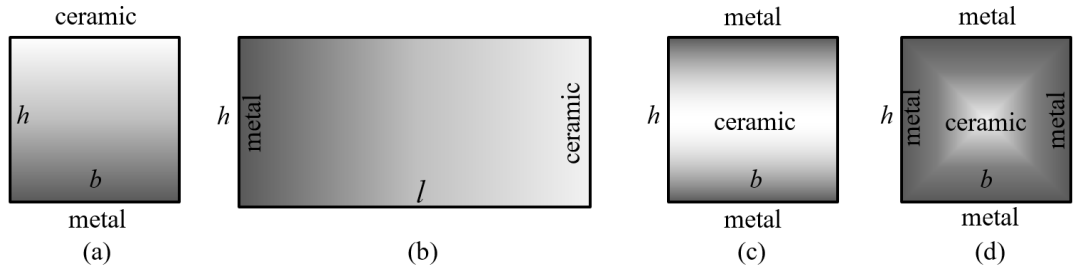

Fig. 3. Beam material gradings (a) HP-beam; (b) LP-beam; (c) HS- beam; (d) HBS- beam.

3. Effective elastoplastic properties

The elastoplastic behavior of the FG beam is described by the TTO scheme. Based on the flow theory of plasticity, this scheme is used to determine the effective material properties of FGMs beyond the elastic limits, where the ceramic ratio is not very dominant [37]. The yield condition can be divided into two parts and written as follows.

$$F(\boldsymbol{\sigma}, \kappa) = f(\boldsymbol{\sigma}) - k(\kappa) = 0 \tag{6}$$

Here, $f(\sigma)$ is the yield criterion, and $k(\kappa)$ is the yield stress curve obtained from uniaxial test data. Experimental observations have shown that the plastic deformation of metals is independent of hydrostatic pressure [38]. Any stress tensor can be divided into hydrostatic and deviatoric parts and expressed as in Eq. 7.

$$\sigma_{ij} = \delta_{ij}\,\sigma_m + \sigma'_{ij} \tag{7}$$

In the above equation, δ_{ij} is the Kronecker delta, $\sigma_m = \sigma_{ii}/3$ is the hydrostatic pressure or mean stress, and σ'_{ij} is the deviatoric stress tensor.

When the yield criterion reaches the yield surface, as in Eq. 7, it remains on the surface with a slight stress increase, and plastic deformation begins. In the updated Lagrangian (UL) formulation, when the effective plastic strain does not exceed 2% [37], the change in total strain can be divided into elastic and plastic parts and expressed as follows.

$$d\boldsymbol{\varepsilon} = d\boldsymbol{\varepsilon}^e + d\boldsymbol{\varepsilon}^p \tag{8}$$

In the flow theory of plasticity, stresses are related to the change in strain. For isotropic materials, according to Hooke's law, the change in the elastic part of the strain can be written as in Eq. 9 related to the change in stress.

$$d\varepsilon^e_{ij} = \frac{d\sigma'_{ij}}{2G} + \frac{(1-2\nu)\delta_{ij} d\sigma_{kk}}{3E} \tag{9}$$

Where $d\sigma'_{ij}$ is the change in deviatoric stress tensor, $d\sigma_{kk}$ is the change in mean stress, G, E and ν are the shear modulus, elastic modulus and Poisson's ratio of the material, respectively. The associated flow rule for deformations of the material in the plastic region is as follows.

$$d\boldsymbol{\varepsilon}^p = d\Lambda \left[\frac{\partial f}{\partial \boldsymbol{\sigma}}\right] \tag{10}$$

Here, $d\Lambda$ is the hardening parameter. $\partial f/\partial \boldsymbol{\sigma}$ corresponds to a vector perpendicular to the yield surface at the corresponding stress point and determines the direction in the flow rule. The following equation can be written by determining the yield criterion according to the J_2 yield criterion.

$$d\varepsilon^p_{ij} = d\Lambda \frac{\partial J_2}{\partial \sigma_{ij}} = d\Lambda\, \sigma'_{ij} \tag{11}$$

In the above equation, J_2 is the second invariant of the deviatoric stress tensor. The effective stress change and effective strain change are as shown in Eq. 12 and Eq.13, respectively.

$$\bar{\sigma} = \sqrt{3 J_2} \tag{12}$$

$$\overline{d\varepsilon}^p = \sqrt{\frac{2}{3}\, d\varepsilon_{ij} d\,\varepsilon_{ij}} \tag{13}$$

The plastic modulus, Ep, relating the stress change and plastic strain change, is expressed as follows.

$$E_p = \frac{d\bar{\sigma}}{d\bar{\varepsilon}^p} = \frac{E E_T}{E - E_T} \tag{14}$$

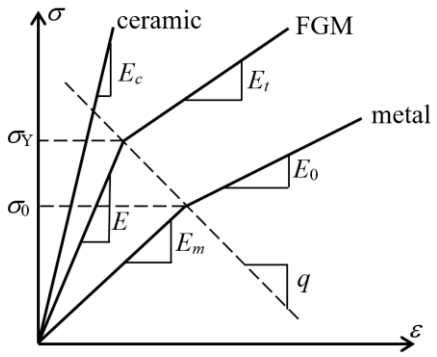

Fig. 4. Bi-linear stress-strain graph according to TTO scheme.

The elastoplastic constitutive equation is written as follows.

$$d\varepsilon_{ij} = \frac{d\,\sigma'_{ij}}{2G} + \frac{(1-2\nu)\delta_{ij}d\sigma_{kk}}{3E} + \frac{3d\overline{\sigma}}{2\overline{\sigma}E_p}\,\sigma'_{ij} \tag{15}$$

In the TTO model, the ceramic material is linearly elastic, as shown in Fig. 4. It is accepted that the functionally graded material will behave according to the J_2 flow theory, as in metals, when the yielding limit is exceeded. According to the model, the uniaxial stress and strain of the graded material with isotropic hardening are related to the volume fraction of the materials [11].

$$\sigma = \sigma_c V_c + \sigma_m V_m \tag{16}$$

$$\varepsilon = \varepsilon_c V_c + \varepsilon_m V_m \tag{17}$$

In above equations σ_c, σ_m ve ε_c, ε_m are the uniaxial stress and strain of the ceramic and metal, respectively. The stress and strain relationship is provided by the modulus denoted by positive definite q. This modulus is written as,

$$q = \frac{\sigma_c - \sigma_m}{|\varepsilon_c - \varepsilon_m|} \tag{18}$$

According to the TTO model, the effective material properties are defined using the material properties forming the FGM, volume fractions, and modulus q as follows.

$$E = \left[E_m V_m \frac{q+E_c}{q+E_m} + E_c V_c\right] / \left[V_m \frac{q+E_c}{q+E_m} + V_c\right] \tag{19}$$

$$\sigma_y = \sigma_0 \left[V_m + \frac{q+E_m}{q+E_c}\frac{E_c}{E_m} V_c\right] \tag{20}$$

$$E_t = \left[E_0 V_m \frac{q+E_c}{q+E_0} + E_c V_c\right] / \left[V_m \frac{q+E_c}{q+E_0} + V_c\right] \tag{21}$$

The effective Poisson's ratio can be written by following the Voigt model as [38],

$$\nu = \nu_c V_c + \nu_m V_m \tag{22}$$

4. Incremental finite element formulation

The notation of formulation used here includes the tensor notation. The lower right indices represent the coordinates in the three-dimensional Euclidean space, taking values from 1 to 3. The comma between the coordinate indices indicates the partial derivative with respect to position. The lower left symbol refers to the reference time step, and the upper left symbol refers to the current time step. The presence of a single superscript on the left indicates that the referenced geometry and the corresponding geometry are the same. The presence of a single subscript and no symbols on the left side describe the quantity change relative to the reference time step and the current time step, respectively. The index appearing twice on only one side of the equation requires the summation convention. The time step corresponds also to the load level since static analysis is performed.

The incremental finite element formulation is based on the solutions of linearized equations for times 0, Δt, $2\Delta t$, t. In case of UL formulation, the variables are referred to the last calculated configuration in the solution. With arbitrarily chosen virtual displacements and displacement boundary conditions satisfied, the principle of virtual displacements requires the following equation for the time $t+\Delta t$ [37].

$$\int_{t_V} {}^{t+\Delta t}_{t}S_{ij}\,\delta\,{}^{t+\Delta t}_{t}\varepsilon_{ij}\,d\,{}^{t}V = {}^{t+\Delta t}\mathcal{R} \tag{23}$$

Here, ${}^{t}V$ is the volume of the continuum, ${}^{t+\Delta t}\mathcal{R}$ is the external virtual work. δ shows that the quantity is virtual. The relation between Green-Lagrange strain tensor, ${}^{t+\Delta t}_{t}\varepsilon_{ij}$, and second Piola-Kirchhoff stress tensor, ${}^{t+\Delta t}_{t}S_{ij}$, is as follows.

$${}^{t+\Delta t}_{t}S_{ij} = {}^{t+\Delta t}_{t}C^{EP}_{ijrs}\,{}^{t+\Delta t}_{t}\varepsilon_{rs} \tag{24}$$

The elements of elastoplastic constitutive tensor ${}^{t+\Delta t}_{t}C^{EP}_{ijrs}$ depends on the location because of the material grading. Since the Second Piola-Kirchhoff stress tensor ${}^{t}_{t}S_{ij}$ for the configuration at time t corresponds to the Cauchy stress tensor ${}^{t}\tau_{ij}$, the Second Piola-Kirchhoff stress tensor in the incremental formulation at time $t+\Delta t$ is written as [37].

$${}^{t+\Delta t}_{t}S_{ij} = {}^{t}\tau_{ij} + {}_{t}S_{ij} \tag{25}$$

The incremental representation of the Green-Lagrange strain tensor and its expression using its linear and nonlinear parts are given below, respectively.

$${}^{t+\Delta t}_{t}\varepsilon_{ij} = {}_{t}\varepsilon_{ij} \tag{26}$$

$${}_{t}\varepsilon_{ij} = {}_{t}e_{i,j} + {}_{t}\eta_{i,j} \tag{27}$$

These linear and nonlinear parts can be written as shown in Eq. 28 and Eq. 29, respectively, using the displacement vector **u** as,

$${}_{t}e_{ij} = \frac{1}{2}({}_{t}u_{i,j} + {}_{t}u_{j,i}) \tag{28}$$

$${}_{t}\eta_{ij} = \frac{1}{2}\,{}_{t}u_{k,i}\,{}_{t}u_{k,j} \tag{29}$$

The equation of motion in virtual displacements principle using the incremental UL formulation becomes as in Eq. 30.

$$\int_{{}^tV} {}_tS_{ij}\,\delta\,{}_t\varepsilon_{ij}\,d^tV + \int_{{}^tV} {}^t\tau_{ij}\,\delta\,{}_t\eta_{ij}\,d^tV = {}^{t+\Delta t}\mathcal{R} - \int_{{}^tV} {}^t\tau_{ij}\,\delta\,{}_te_{ij}\,d^tV \tag{30}$$

The linearized equation of motion can be written using the approximations ${}_tS_{ij}={}_tC_{ijrs}\,{}_te_{rs}$ and ${}_t\varepsilon_{ij} = {}_te_{ij}$ as,

$$\int_{{}^tV} {}_tC^{EP}_{ijrs}\,{}_te_{rs}\,\delta\,{}_te_{ij}\,d^tV + \int_{{}^tV} {}^t\tau_{ij}\,\delta\,{}_t\eta_{ij}\,d^tV = {}^{t+\Delta t}\mathcal{R} - \int_{{}^tV} {}^t\tau_{ij}\,\delta\,{}_te_{ij}\,d^tV \tag{31}$$

This equation is fundamental in isoparametric finite element analysis [37]. Since external loads are torsional loads, the applied load follows the deformations and is updated at each solution step, as shown in Fig. 5.

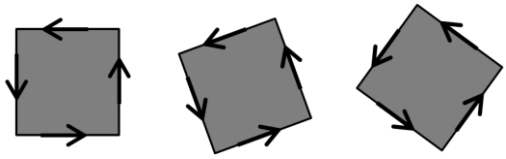

Fig. 5. Representation of loads following the deformation.

$$h_k = (1+\xi\xi_k)(1+\eta\eta_k)(1+\zeta\zeta_k)/8 \tag{32}$$

In above equation, k=1, 2, …, 8 represents the node numbers of hexahedral finite element, as shown in Fig. 6. ξ, η, ζ are isoparametric coordinates and ξ_k, η_k, ζ_k = ±1. Linear and nonlinear strain-displacement transformation matrices, ${}^t_t\mathbf{B}_L$ ve ${}^t_t\mathbf{B}_{NL}$, can be written by taking partial derivatives with respect to the coordinates as in Eq. 33 and Eq. 34.

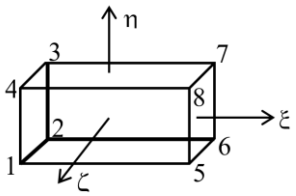

Fig. 6. Isoparametric finite element.

$${}^t_t\boldsymbol{B}_L = \begin{bmatrix} {}_th_{1,1} & 0 & 0 & {}_th_{2,1} & \dots & 0 \\ 0 & {}_th_{1,2} & 0 & 0 & \dots & 0 \\ 0 & 0 & {}_th_{1,3} & 0 & \dots & {}_th_{m,3} \\ {}_th_{1,2} & 0 & 0 & {}_th_{2,2} & \dots & 0 \\ 0 & {}_th_{1,3} & {}_th_{1,2} & 0 & \dots & {}_th_{m,2} \\ {}_th_{1,3} & 0 & {}_th_{1,1} & {}_th_{2,3} & \dots & {}_th_{m,1} \end{bmatrix} \tag{33}$$

$$ {}_{t}^{t}\boldsymbol{B}_{NL} = \begin{bmatrix} {}_{t}^{t}\widetilde{\boldsymbol{B}}_{NL} & \widetilde{\mathbf{0}} & \widetilde{\mathbf{0}} \\ \widetilde{\mathbf{0}} & {}_{t}^{t}\widetilde{\boldsymbol{B}}_{NL} & \widetilde{\mathbf{0}} \\ \widetilde{\mathbf{0}} & \widetilde{\mathbf{0}} & {}_{t}^{t}\widetilde{\boldsymbol{B}}_{NL} \end{bmatrix} \tag{34} $$

where,

$$ {}_{t}^{t}\widetilde{\boldsymbol{B}}_{NL} = \begin{bmatrix} {}_{t}h_{1,1} & 0 & 0 & \cdots & {}_{t}h_{m,1} \\ {}_{t}h_{1,2} & 0 & 0 & \cdots & {}_{t}h_{m,2} \\ {}_{t}h_{1,3} & 0 & 0 & \cdots & {}_{t}h_{m,3} \end{bmatrix} \tag{35} $$

The linearized version of equation of motion given in Eq. 31 becomes,

$$ \underbrace{\left(\int_{t_V} {}_{t}^{t}\boldsymbol{B}_{L}^{T}\ {}_{t}\boldsymbol{C}^{EP}\ {}_{t}^{t}\boldsymbol{B}_{L}\, d^{t}V\right)\widehat{\boldsymbol{u}}}_{{}_{t}^{t}\boldsymbol{K}_{L}\widehat{\boldsymbol{u}}} + \underbrace{\left(\int_{t_V} {}_{t}^{t}\boldsymbol{B}_{NL}^{T}\ {}^{t}\boldsymbol{\tau}\ {}_{t}^{t}\boldsymbol{B}_{NL}\, d^{t}V\right)\widehat{\boldsymbol{u}}}_{{}_{t}^{t}\boldsymbol{K}_{NL}\widehat{\boldsymbol{u}}} = {}^{t+\Delta t}\boldsymbol{R} - \underbrace{\int_{t_V} {}_{t}^{t}\boldsymbol{B}_{L}^{T}\ {}^{t}\widehat{\boldsymbol{\tau}}\, d^{t}V}_{{}_{t}^{t}\boldsymbol{F}} } \tag{36} $$

where ${}_{t}\mathbf{C}^{EP}$ is the incremental elastoplastic constitutive matrix and ˆ represents vectors. Since the virtual displacements can be chosen as arbitrary unit vectors, they can be eliminated from the equation. The integrals were calculated using Gauss quadrature method with Gauss integration order of n=3 and each finite element has 27 Gauss integration points. The effective material properties due to the material grading were calculated at each Gauss integration point. Finite element formulation in Eq. 36 can be written as,

$$ ({}_{t}^{t}\boldsymbol{K}_{L} + {}_{t}^{t}\boldsymbol{K}_{NL})\boldsymbol{U} = {}^{t+\Delta t}\boldsymbol{R} - {}_{t}^{t}\boldsymbol{F} \tag{37} $$

where ${}_{t}^{t}\mathbf{K}_{L}$ and ${}_{t}^{t}\mathbf{K}_{NL}$ are linear and nonlinear strain incremental stiffness matrices, respectively. ${}_{t}^{t}\mathbf{F}$ are nodal point loads at time t and ${}^{t+\Delta t}\mathbf{R}$ is deformation following external forces. The unknown displacements in Eq. 37 were calculated using Newton-Raphson and modified Newton-Raphson iteration methods together.

5. Numerical analysis

A code in Java SE [39] programming language was developed in the Netbeans [40] environment in order to perform numerical analyses. The code produces the result with the formulation given above. Three-dimensional visualization of the plastic region propagation was carried out through the code created in the Matlab [41] environment.

The reliability of the code developed based on the given formulation was determined by comparing the work of Nguyen et al. [42], examining the nonlinear bending behavior of elastoplastic FG beams. The clamped beam shown in Fig. 7 is functionally graded from ceramic to metal using the power law in the height direction. Axial stress values were compared at points P1 and P2 shown on the beam with their coordinates on Fig. 7. Different power law distribution parameter values (n) were used in this comparison. Additionally, two different external load values were used. The results are shown in Table 1. The maximum difference between stresses was calculated as 4.5%. In the normalized load - dimensionless displacement graph shown in Fig. 8, the difference between the maximum dimensionless displacements is 4.6%.

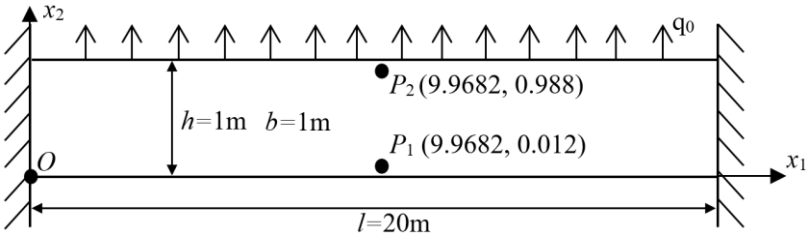

Fig. 7. Problem geometry used in comparison [42].

Table 1. Axial stresses under uniformly distributed load (MPa).

		q_0 (kN/m)					
		1500			3500		
n	Point	Code	Nguyen et al. [42]	Difference %	Code	Nguyen et al. [42]	Difference %
0.5	P_1	-95.59	-92.83	2.97	-219.85	-213.43	3.01
0.5	P_2	208.64	216.40	3.58	493.81	512.67	3.68
2	P_1	-113.97	-114.96	0.86	-262.62	-266.12	1.31
2	P_2	258.26	268.52	3.82	602.18	628.08	4.12
5	P_1	121.94	-122.83	0.72	-282.63	-287.43	1.67
5	P_2	295.64	309.56	4.49	651.76	681.06	4.30

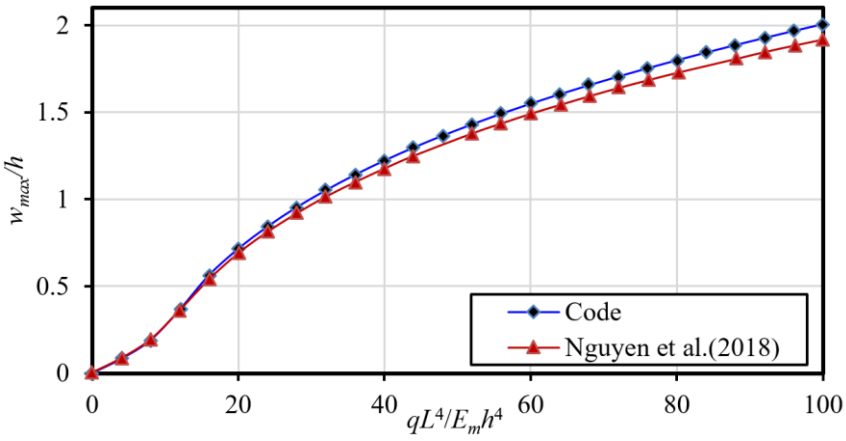

Fig. 8. Variation of maximum dimensionless displacement with normalized load [42].

5.1. Functionally graded square section beam

The torsion behavior of the functionally graded beams given in Section 1 has been examined numerically. The dimensions of the beam shown in Fig. 9 are b = 210 mm, h = 210 mm, and l = 1440 mm. Torsional loading was applied using deformation-following forces located on the rigid elements. Since axial displacements are not prevented, plane sections no longer remain plane. The section corresponding to the x_1=0 plane, where the load is

applied to the FG beam, is named CS1. The behavior was examined by applying a torsional loading that would cause this section to rotate around the longitudinal axis by $\phi = 12.5°$. Stress values were read in Gaussian points. At each load step, the load increment that would create the same angular deformation increment was calculated by extrapolation and applied to the system.

1617 finite elements were used in the analysis. Finite element dimensions are b_e=30 mm, h_e=30 mm, and l_e=45 mm. 2176 nodal points and 43659 Gauss integral points were created.

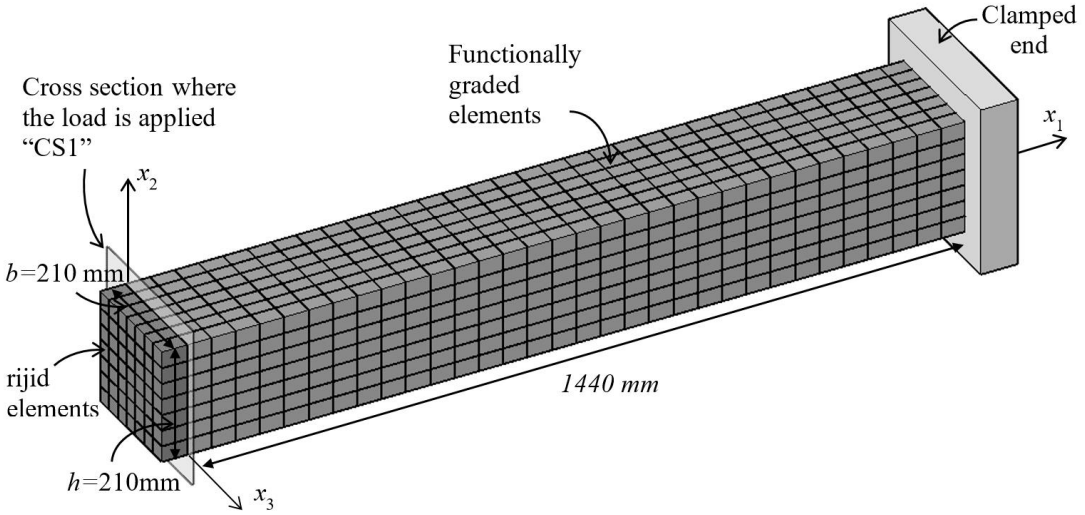

Fig. 9. Finite element model used in numerical analysis.

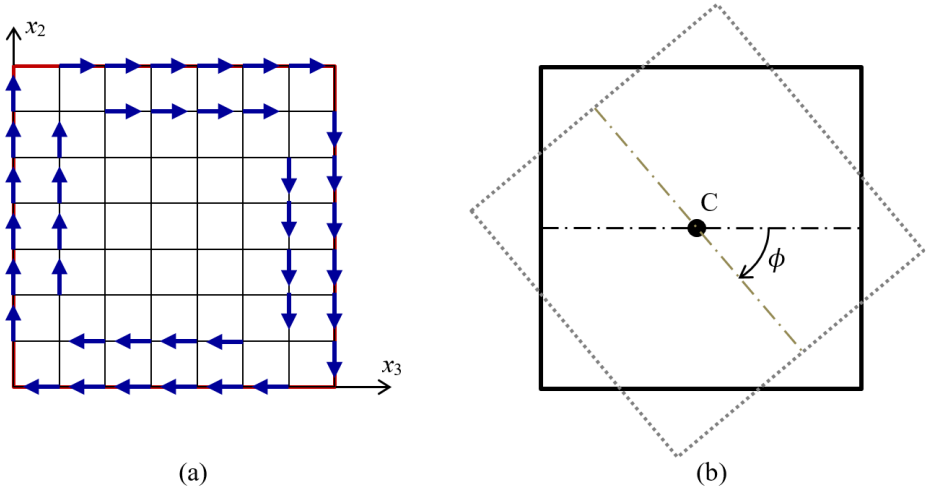

Fig. 10. (a) Loading to create torsional moment; (b) Angle of rotation.

In the beam with one end clamped, the loads deformation-following loading were applied as concentrated forces on the nodes in the CS1 section at the free end, as shown in Fig. 10a. Thus, a torsional moment is created.

Elastoplastic properties for the TiB-Ti (Titanium Boride-Titanium) material used in the analysis [12] are E_c=375 GPa (TiB), E_m=107 GPa (Ti), E_0=14 GPa, σ_0=450 MPa, q=4.5 GPa, ν_m=0.34, and ν_c=0.14. Rigid elements were considered as linear elastic and their mechanical properties are E=50000 GPa and ν=0.001.

The variation of the normalized load with the angle of rotation of the CS1 section is shown in Fig. 11 for different beam gradings. With the onset of plastic deformation, the loading-rotation angle graph slope decreases. The decrease in the slope of the graph started when 80% of the total load level was reached for the all-metal beam. The decrease in the slope of the graph started when the load level reached approximately 60% for the HP-beam. For other beams, a decrease in the slope of the graph was observed between these two values. In Appendix A, the propagation of the plastic region in the beams is shown in detail by visualizing the results for different rotation angles. The HP beam with the largest torsional stiffness starts plastic deformation at the smallest rotation angle. In the metal beam with the lowest torsional stiffness, the plastic flow starts at large rotation angle.

Table 2. Torsional moment values versus the angle (ϕ) formed at CS1 section.

FD beam torsional moment (kNm)					
ϕ	Metal	HP n=1	LP n=1	HS	HBS
0.5	58.06	107.26	96.73	97.25	88.53
1.0	116.13	214.52	193.47	194.50	177.07
1.5	174.19	321.20	290.20	291.75	265.60
2.0	232.25	424.60	386.93	388.12	354.13
2.5	290.32	518.61	481.89	480.41	442.66
3.0	348.38	598.32	559.60	566.71	531.19
3.5	406.44	666.31	614.80	646.09	615.30
4.0	463.94	723.16	657.55	713.31	665.56
4.5	514.35	770.65	690.51	757.59	695.36
5.0	555.27	812.31	718.52	789.48	720.52
5.5	588.49	849.16	742.98	817.26	744.00
6.0	616.12	882.19	765.53	842.97	764.81
6.5	639.56	913.42	786.14	866.62	783.40
7.0	659.62	943.28	805.48	888.84	801.25
7.5	675.80	971.46	823.90	910.14	818.31
8.0	691.30	998.91	841.68	930.55	834.61
8.5	704.96	1025.84	858.79	950.78	850.56
9.0	717.41	1052.13	875.48	970.90	866.25
9.5	729.18	1078.11	891.88	990.92	881.90
10.0	740.79	1103.70	908.03	1010.81	897.46
10.5	751.62	1128.92	923.99	1030.63	912.93
11.0	761.65	1153.79	939.81	1050.37	928.33

11.5	771.38	1178.36	955.52	1069.98	943.71
12.0	780.72	1202.71	971.13	1089.48	959.05
12.5	789.91	1226.94	986.65	1108.89	974.36

Torsional moments corresponding to the rotation angle ϕ in the CS1 section, obtained by grading with different functions for beams with equal amounts of metal and ceramic materials in total, are given in Table 2. The moment value required to create the same angle of twist was highest for the HP-beam. As the ceramic ratio on the outer walls increases and the effective material modulus of elasticity increases, the resistance to torsion increases. The HP-beam is followed by the HS-beam. Among the FG beams graded on the transverse cross-section, the HBS-beam, which has metal on all four outer walls and turns to ceramic towards the middle of the section, shows the lowest resistance to torsion.

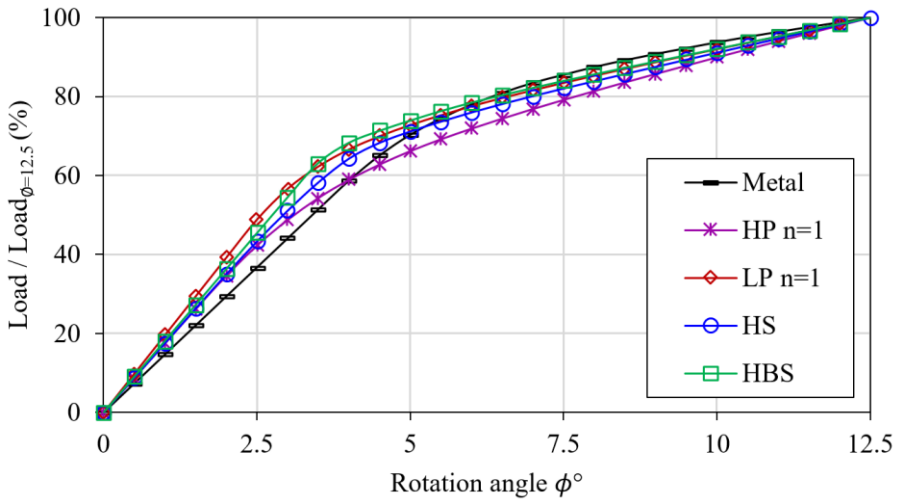

Fig. 11. Variation of the normalized load with the rotation angle of the beam end.

The torsion-induced angular deformation along the FG beam, from CS1 section to the clamped end, for ϕ=12.5° is given in Fig. 12. For beams made of pure metal and graded in the cross-sectional plane, the angle variation along the beam is linear, whereas for LP-beams the variation is non-linear. In these beams, the angle variation along the beam for different values of n is also non-linear as shown in Fig. 13, and the curvature of the graph increases with increasing ceramic content in the beam. If the ceramic volume fraction increases in a section, the angle of rotation decreases.

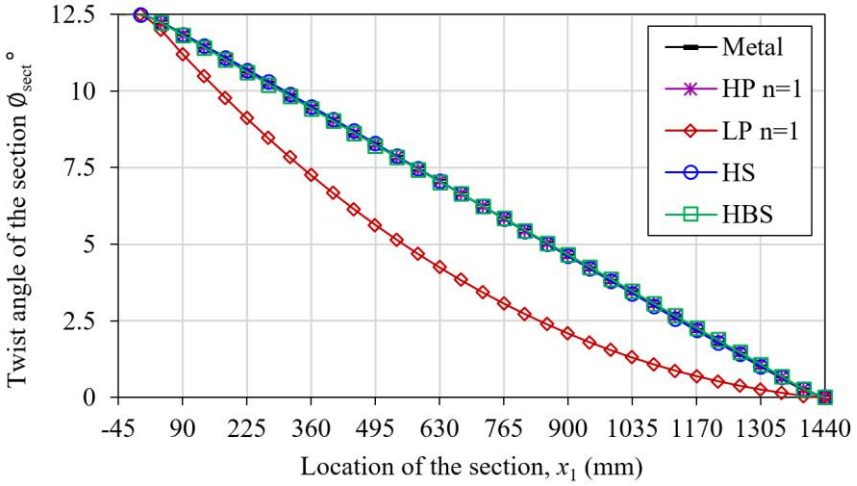

Fig. 12. Variation of angle of twist along the beam length for different FG beams.

In the region where torsional load is applied on FG beams, the change of s_{12} shear stresses in the x_3 direction for ϕ=12.5° at Gaussian points on the horizontal line passing through the center of the section (x_2=105 mm) is given in Fig. 14. Unlike homogeneous beams, in functionally graded beams, there are cases where the largest shear stresses do not occur at the outer boundaries of the section. In the HBS-beam, the largest shear stresses occur in the inner region of the section. Fig. 15 shows that the largest s_{13} shear stresses read at the Gaussian points on the vertical line passing through the center of the same section (x_3=105 mm) do not occur at the outer boundaries of the section for HBS- and HS-beams. This behavior, which is different from homogeneous beams, can also be seen in the s_{12} shear stress values read at the Gaussian points on the diagonal of the section in this region as shown in Table 3.

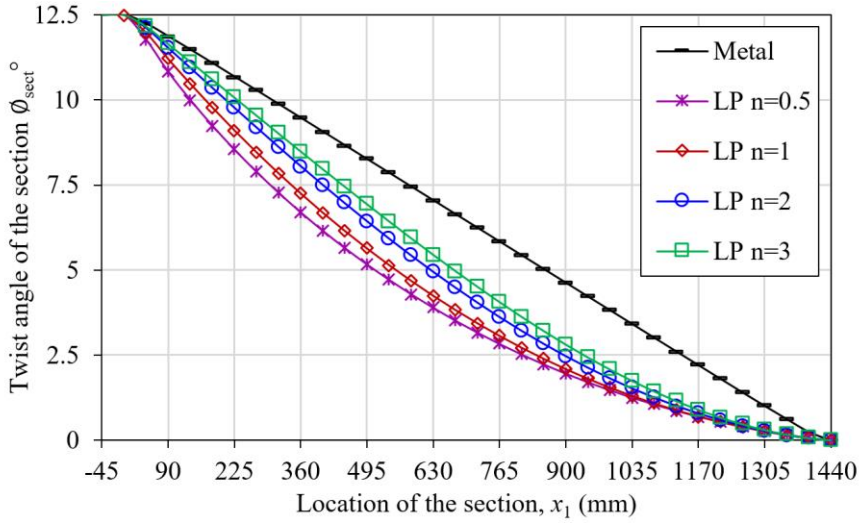

Fig. 13. Variation of angle of twist along the beam length for LP-beams.

Table 3. s_{12} shear stress values at Gaussian points on the cross-section diagonal for ϕ=12.5° in the region where the load is applied.

Coordinates (mm)				s_{12} shear stress (MPa)				
Point	x_1	x_2	x_3	Metal	HP n=1	LP n=1	HS	HBS
1	5.072	3.381	3.381	180.398	142.221	214.506	191.653	183.971
2	5.072	26.619	26.619	170.765	140.885	199.092	179.993	186.106
3	5.072	33.381	33.381	170.689	141.063	197.798	181.179	192.598
4	5.072	56.619	56.619	159.782	123.158	179.359	166.570	206.610
5	5.072	63.381	63.381	158.174	115.967	175.330	162.131	216.493
6	5.072	86.619	86.619	71.646	66.484	151.111	157.045	224.011
7	5.072	105.0	105.0	0.0	-38.559	0.0	0.0	0.0
8	5.072	123.381	123.381	-71.646	-204.215	-151.111	-157.045	-224.011
9	5.072	146.619	146.619	-158.174	-284.833	-175.330	-162.131	-216.493
10	5.072	153.381	153.381	-159.782	-292.982	-179.359	-166.570	-206.610
11	5.072	176.619	176.619	-170.689	-395.976	-197.798	-181.179	-192.598
12	5.072	183.381	183.381	-170.765	-419.03	-199.092	-179.993	-186.106
13	5.072	206.619	206.619	-180.398	-1156.22	-214.506	-191.653	-183.971

In the HP-beam, unlike other FG beams and the metal beam, shear stresses are not zero at the center of the section geometry, as seen in Fig. 14 for s_{12} and in Fig. 15 for s_{13}. This can also be seen for point 7 on the HP-beam in Table 3. The shift of the point where the stress is zero increases as the power law distribution coefficient (n) changes to increase the ceramic ratio, as shown in Fig. 16.

This situation occurs when the cross-section is not symmetric in terms of volume fractions with respect to both horizontal and vertical axes. This causes the section to behave as a geometrically non-symmetrical section. The shear center is no longer the geometric center of the section. As shown in Fig. 17, the cross-section is displaced in the transverse direction, in the direction of the material gradation relative to the initial position, towards the material with smaller effective material properties. Unlike other beams, these transverse displacement values in the HP-beam can reach 3% of the section height, as seen in Fig.18.

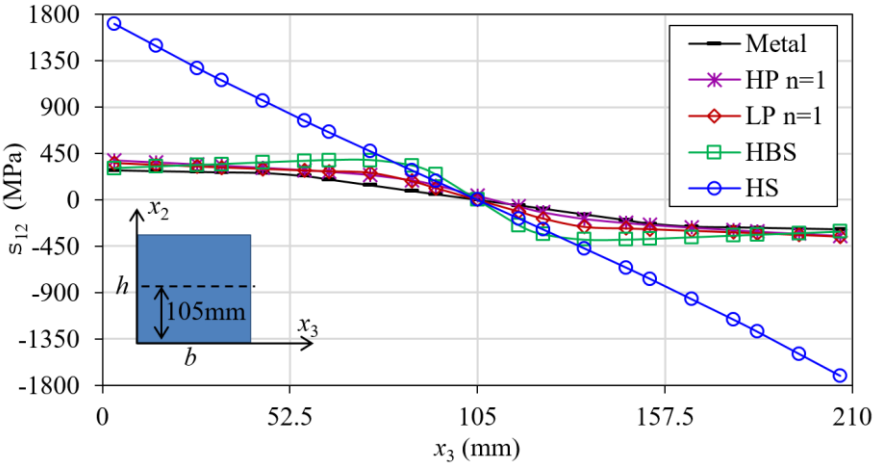

Fig. 14. Variation of shear stress (s_{12}) at x_2=105 mm with x_3 in the loading region.

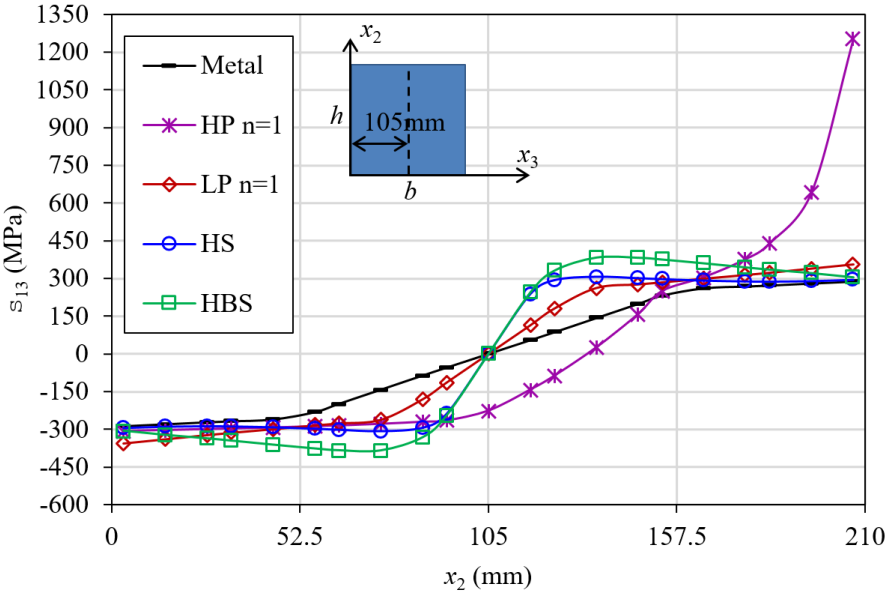

Fig. 15. Variation of shear stress (s_{13}) at x_3=105 mm with x_2 in the loading region.

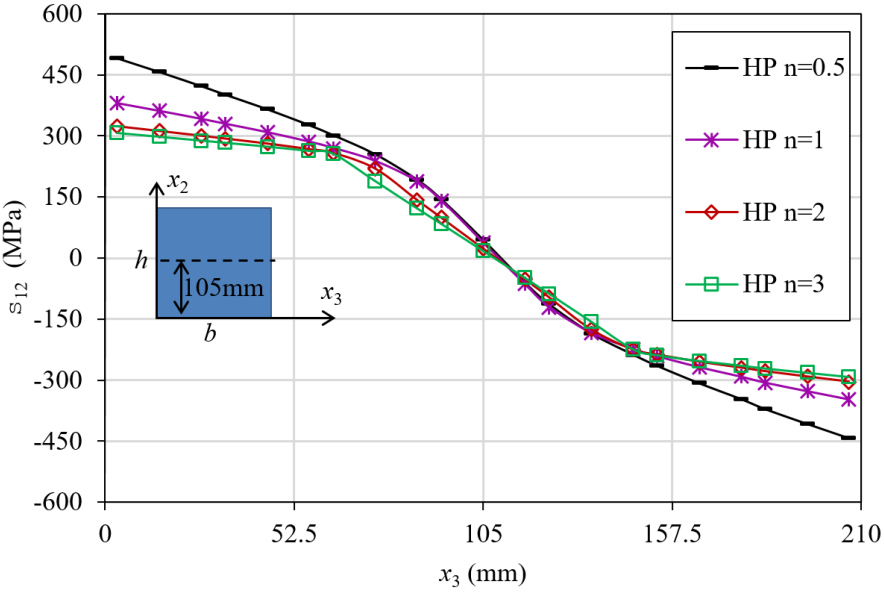

Fig. 16. Variation of shear stress (s_{12}) at x_2=105 mm with x_3 in the loading region for HP-beams.

Fig. 19 shows the axial displacements at the nodes on the diagonal of the CS1 section for the rotation angle of ϕ=12.5°. The distribution of axial displacements in sections that are symmetrical with respect to any axis within the section is similar to a homogeneous metal beam. Axial displacements tend to decrease towards the middle of the section in the homogeneous beam. In the HP-beam, they are high in regions where the metal ratio is high and low in regions where the ceramic ratio is high.

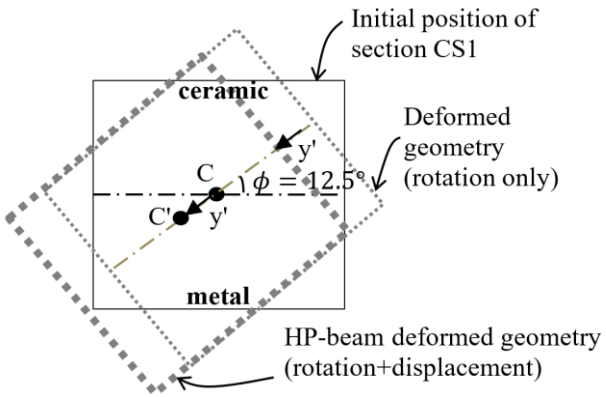

Fig. 17. CS1 section transverse displacement in the direction of material gradation for HP-beams.

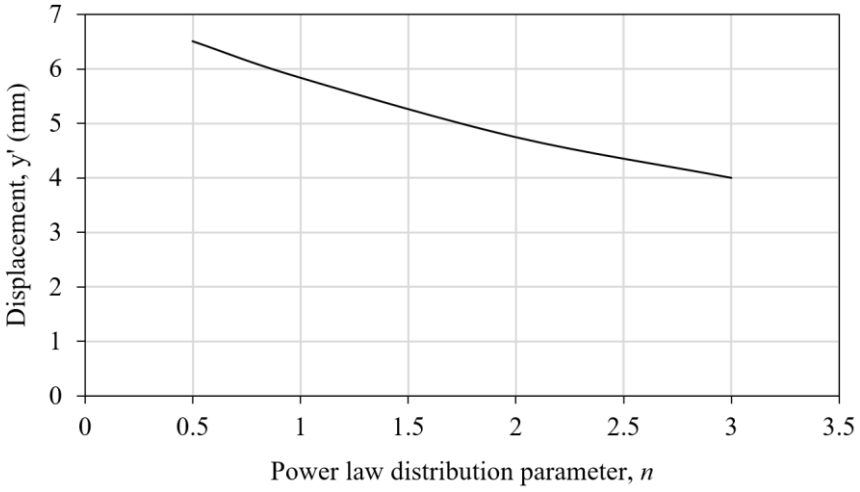

Fig. 18. HP-beam CS1 section transverse displacement, y' (mm), for different *n* values at ϕ=12.5°.

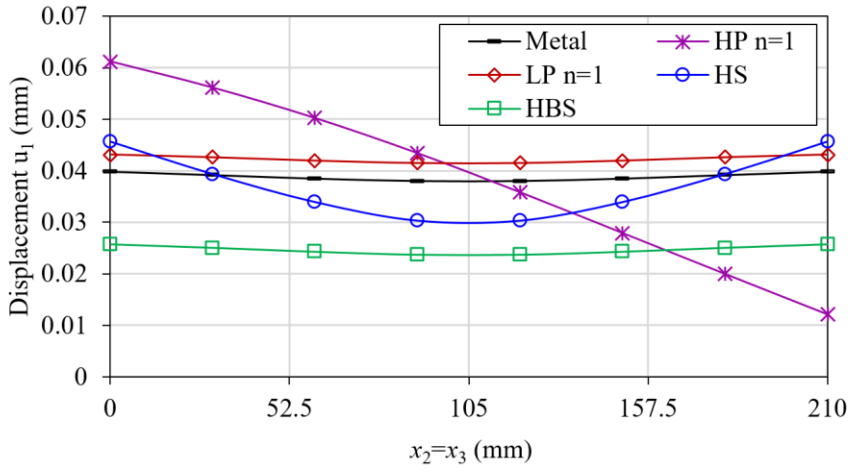

Fig. 19. Axial displacements at points on the cross-section diagonal for $\phi = 12.5°$ in CS1 section.

6. Conclusion

The torsional behavior of functionally graded ceramic-metal elastoplastic beams was investigated using the nonlinear finite element method. Effective elastoplastic properties were obtained using the TTO scheme. The nonlinear finite element formulation was created with the updated Lagrangian formulation based on the virtual displacement principle. An iterative solution based on Newton-Raphson and updated Newton-Raphson methods was used to solve the nonlinear equation system. Effective material properties were calculated at Gaussian points.

The torsional behavior of FG beams differs from homogeneous beams depending on the material distribution used. According to the material distribution, the largest shear stresses are not at the outer boundaries of the section, unlike the homogeneous beam. In the FG beam, graded from metal to ceramic from outer walls towards the middle

of the section, with a sinusoidal function, the largest shear stresses occur in the region close to the mid-region of the section. The HP-beam, which is graded from ceramic to metal in the direction of the cross-section height according to the power law, is displaced in the transverse direction relative to its initial position under torsional loads, unlike the homogeneous beam and the FG beams that have two or more symmetries in the section plane. In addition, shear stresses are not zero in the center of the section. In the LP-beam with material grading along the longitudinal direction, the change of the rotation angle along the beam, unlike other beams, is not linear and varies according to the material distribution.

The distribution of the plastic regions in FG beams was also examined for different material distributions. Although the distribution of the plastic region in the LP-beam graded in the axial direction is similar to the homogeneous beam, in the beams graded in the section plane, the distribution of the plastic region varies depending on the material distribution. The plastic region shifts towards ceramic-dense regions with higher effective Young modulus. However, yielding begins close to the outer boundaries of the section.

Acknowledgements

This research received no specific grants from any funding agency in public, commercial or non-profit sectors.

References

[1] M. Koizumi, "FGM activities in Japan," *Composites Part B*, vol. 28, no. 1, pp. 1-4, 1997, doi: 10.1016/S1359-8368(96)00016-9.
[2] T. Hirai, "Functional gradient materials," in. *Materials Science and Technology*, 3 b., vol. 17B, R. J. Brook, Ed., Weinheim, VCH Verlagsgesellschaft mbH, 1996, pp. 293-341.
[3] S. H. Chi and Y. L. Chung, "Mechanical behavior of functionally graded material plates under transverse load-Part I: Analysis," *International Journal of Solids and Structures*, vol. 43, no. 13, pp. 3657-3674, June 2006, doi: 10.1016/j.ijsolstr.2005.04.011.
[4] F. Tornabene and E. Viola, "Free vibrations of four-parameter functionally graded parabolic panels and shells of revolution," *European Journal of Mechanics A/Solids*, vol. 28, no. 5, pp. 991-1013, Sept. 2009, doi: 10.1016/j.euromechsol.2009.04.005.
[5] V. Boggarapu, R. Gujjala, S. Ojha, S. Acharya, P. V. Babu, S. Chowdary and D. k. Gara, "State of the art in functionally graded materials," *Composite Structures*, vol. 262, p. 113596, April 2021, doi: 10.1016/j.compstruct.2021.113596.
[6] R. Hill, "A self-consistent mechanics of composite materials", *J. Mech. Phys. Solids*, vol. 13, no. 4, pp. 213-222, Aug. 1965, doi: 10.1016/0022-5096(65)90010-4.
[7] T. Mori and K. Tanaka, "Average stress in matrix and average elastic energy of materials with misfitting inclusions," *Acta Metallaugica*, vol. 21, no. 5, pp. 571-574, May 1973, doi: 10.1016/0001-6160(73)90064-3.
[8] M. M. Gasik and K. R. Lilius, "Evaluation of properties of W-Cu functional gradient materials by micromechanical model," *Computational Materials Science*, vol. 3, no. 1, pp. 41-49, Sept. 1994, doi: 10.1016/0927-0256(94)90151-1.
[9] T. Reiter and G. J. Dvorak, "Micromechanical models for graded composite materials: II. thermomechanical loading," *J. Mech. Phys. Solids*, vol. 46, no. 9, pp. 1655-1673, Sept. 1998, doi: 10.1016/S0022-5096(97)00039-2.
[10] I. Tamura, Y. Tomota and H. Ozawa, "Strenght and ductility of Fe-Ni-C alloys composed of austenite and martensite with various strenght," *Proceeding of the Third International Conference on Strenght of Metals and Alloys*, Cambridge Institute of Metals, vol. 1, pp. 611-615, 1973.
[11] R. L. Williamson, B. H. Rabin and J. T. Drake, "Finite element analysis of thermal residual stresses at graded ceramic metal interfaces. Part I. Model description and geometrical effects," *Journal of Applied Physics*, vol. 74, pp. 1310-1320, July 1993, doi: 10.1063/1.354910.
[12] H. Huang and Q. Han, "Elastoplastic buckling of axially loaded functionally graded material cylindrical shells," *Composite Structures*, vol. 117, pp. 135-142, Nov. 2014, doi: 10.1016/j.compstruct.2014.06.018.
[13] Y. Zhang, H. Huang and Q. Han, "Buckling of elastoplastic functionally graded cylindrical shells under combined compression and pressure," *Composites: Part B*, vol. 69, pp. 120-126, Feb. 2015, doi: 10.1016/j.compositesb.2014.09.024.
[14] H. Zafarmand and M. Kadkhodayan, "Nonlinear material and geometric analysis of thick functionally graded plates with nonlinear strain hardening using nonlinear finite element method," *Aerospace Science and Technology*, vol. 92, pp. 930-944, Sept. 2019, doi: 10.1016/j.ast.2019.07.015.
[15] F. J. Rooney and M. Ferrari, "Torsion and flexure of inhomogeneous elements," *Composites Engineering*, vol. 5, no. 7, pp. 901-911, 1995, doi: 10.1016/0961-9526(95)00043-M.
[16] C. O. Horgan and A. M. Chan, "Torsion of functionally graded isotropic linearly elastic bars," *Journal of Elasticity*, vol. 52, pp. 181-199, Aug. 1998, doi: 10.1023/A:1007544011803.
[17] C. O. Horgan, "On the torsion of functionally graded anisotropic linearly elastic bars," *IMA Journal of Applied Mathematics*, vol. 72, pp. 556-562, Oct. 2007, doi: 10.1093/imamat/hxm027.
[18] R. C. Batra, "Torsion of a functionally graded cylinder," *AIAA Journal*, vol. 44, no. No.6, pp. 1363-1365, June 2006, doi: 10.2514/1.19555.
[19] U. Anita, "Implementation of the method of fundamental solutions and homotopy analysis method for solving a torsion problem of a rod

made of functionally graded material," *Advanced Materials Research,* vols. 123-125, pp. 551-554, Aug. 2010, doi: 10.4028/www.scientific.net/AMR.123-125.551.
[20] M. R. Hematiyan and E. Estakhrian, "Torsion of functionally graded open-section members," *International Journal of Applied Mechanics,* vol. 4, no. 2, p. 1250020, June 2012, doi: 10.1142/S1758825112500202.
[21] T. T. Nguyen, N. I. Kim and J. Lee, "Analysis of thin-walled open-section beams with functionally graded materials," *Composite Structures,* vol. 138, pp. 75-83, March 2016, doi: 10.1016/j.compstruct.2015.11.052.
[22] I. Ecdesi and A. Baksa, "Torsion of Functionally Graded Anisotropic Linearly Elastic Circular Cylinder," *Engineering Transactions,* vol. 66, no. 4, pp. 413-426, 2018, doi: 10.24423/EngTrans.923.20181003.
[23] G. J. Nie, A. Pydah and R. C. Batra, "Torsion of bi-directional functionally graded truncated conical cylinders," *Composite Structures,* vol. 210, pp. 831-839, Feb. 2019, doi: 10.1016/j.compstruct.2018.11.081.
[24] E. T. Akinlabi, M. N. Mikhin and E. V. Murashkin, "Functionally graded prismatic triangular rod under torsion," *Journal of Physics: Conf. Series,* vol. 1474, p. 012003, 2020, doi: 10.1088/1742-6596/1474/1/012003.
[25] I. Ecsedi, "Non-uniform torsion of functionally graded anisotropic bar of an elliptical cross section," *Acta Mech,* vol. 231, pp. 2947-2953, July 2020, doi: 10.1007/s00707-020-02682-y.
[26] G. C. Tsiatas and N. G. Babouskos, "Elastic-plastic analysis of functionally graded bars under torsional loading," *Composite Structures,* vol. 176, pp. 254-267, Sept. 2017, doi: 10.1016/j.compstruct.2017.05.044.
[27] M. Aminbaghai, J. Murin, V. Kutis, J. Hrabovsky, M. Kostolani and H. A. Mang, "Torsional warping elastostatic analysis of FGM beams with longitudinally varying material properties," *Engineering Structures,* vol. 200, p. 109694, Dec. 2019, doi: 10.1016/j.engstruct.2019.109694.
[28] P. K. Singh, M. Kumar and S. Mishra, "Finite element analysis of functionally graded bar under torsional load," *Materials Today: Proceedings,* vol. 56, pp. 2960-2966, 2022, doi: 10.1016/j.matpr.2021.11.012.
[29] X. Chen, G. Nie and Z. Wu, "Non-uniform torsion analysis of functionally graded beams with solid or thin-walled section using hierarchical Legendre expansion functions," *Mechanics of Advanced Materials and Structures,* vol. 29, no. 14, pp. 2074-2097, 2022, doi: 10.1080/15376494.2020.1851828.
[30] E. Mahmoodi and P. Malekzadeh, "Analytical solutions of multiple cracks and cavities in a rectangular cross-section bar coated by a functionally graded layer under torsion," *Arch Appl Mech,* vol. 91, pp. 2189-2209, May 2021, doi: 10.1007/s00419-020-01877-y.
[31] I. Ecdesi and A. Baksa, "Saint-Venant torsion of functional graded orthotropic piezoelectric hollow circular cylinder," *International Journal on Applied Physics and Engineering,* vol. 2, pp.22-27, 2023, doi: 10.37394/232030.2023.2.4.
[32] F. Mehralian and Y. T. Beni, "Size-dependent torsional buckling analysis of functionally graded cylindrical shell," *Composites,* vol. Part B, no. 94, pp. 11-25, June 2016, doi: 10.1016/j.compositesb.2016.03.048.
[33] T.-T. Nguyen, P. T. Thang and J. Lee, "Flexural-torsional stability of thin-walled functionally graded open-section beams," *Thin-Walled Structures,* vol. 110, pp. 88-96, Jan. 2017, doi: 10.1016/j.tws.2016.09.021.
[34] Y. Wang, C. Feng, Z. Zhao, F. Lu and J. Yang, "Torsional buckling of graphene platelets (GPLs) reinforced functionally graded cylindrical shell with cutout," *Composite Structures,* vol. 197, pp. 72-79, Aug. 2018, doi.org/10.1016/j.compstruct.2018.05.056.
[35] M. Bocciarelli, G.Bolzon and G.Maier, "A constitutive model of metal-ceramic functionally graded material behavior: Formulation and parameter identification," *Computational Materials Science,* vol. 43, pp. 16-26, July 2008, doi: 10.1016/j.commatsci.2007.07.047.
[36] D. Owen and E. Hinton, *Finite Elements in Plasticity: Theory and practice*. Swansea: Pineridge Press Limited, 1980.
[37] K.-J. Bathe, *Finite Element Procedures*. New Jersey: Prentice-Hall Inc., 1996.
[38] Z.-H. Jin, G. H. Paulino and R. H. D. Jr., "Cohesive fracture modeling of elastic-plastic crack growth in functionally graded materials," *Engineering Fracture Mechanics,* vol. 70, no. 14, pp. 1885-1912, Sept. 2003, doi: 10.1016/S0013-7944(03)00130-9.
[39] Oracle Corporation, *JAVA SE*. Version 18.0.0, Programming Language.
[40] The Apache Software Foundation, *NETBEANS IDE*. Version 13, Integrated Development Environment.
[41] The Math Works Inc., *MATLAB*. Version 2023a, Computer Software.
[42] D. K. Nguyen, K. V. Nguyen, V. M. Dinh, B. S. Gan and S. Alexandrow, "Nonlinear bending of elastoplastic functionally graded ceramic-metal beams subjected to nonuniform distributed loads," *Applied Mathematics and Computation,* vol. 333, pp. 443-459, Sept. 2018, doi: 10.1016/j.amc.2018.03.100.

Appendix A. Plastic region propagation

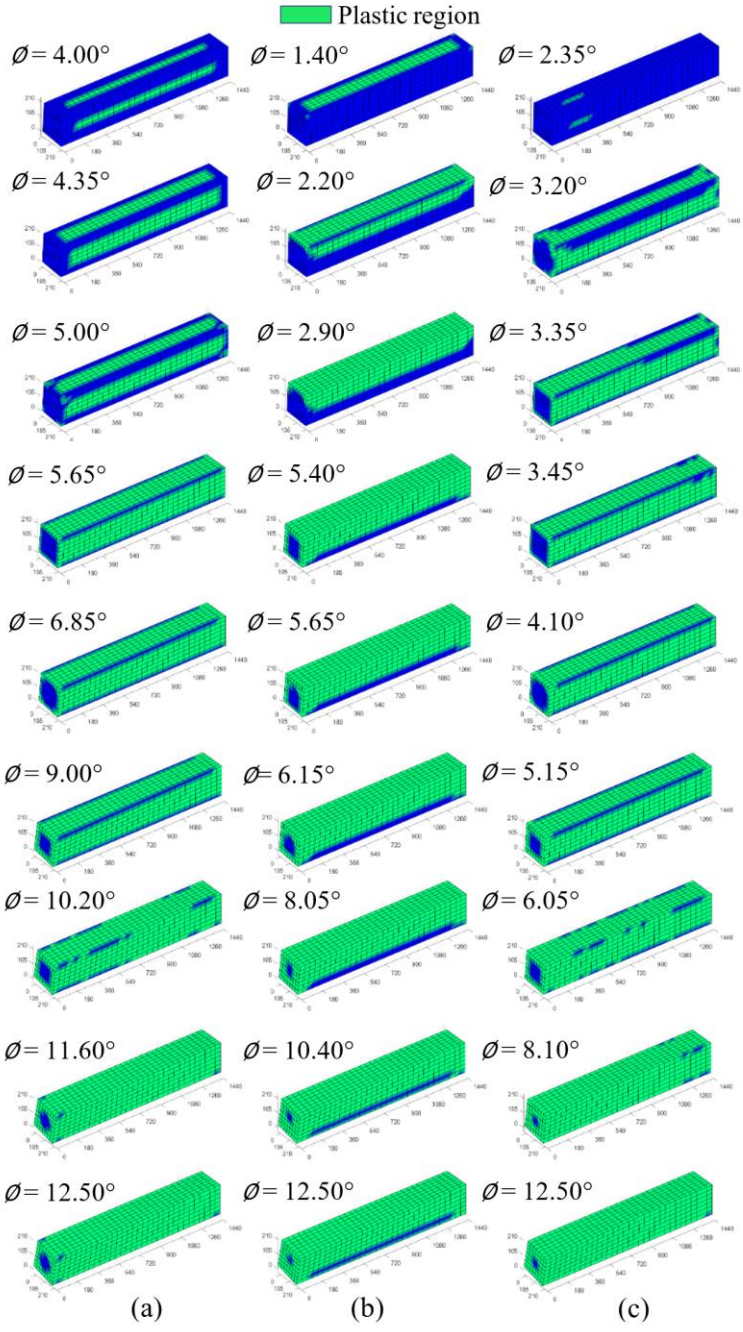

Fig. A1. Distribution of plastic regions in FG beams (a) metal; (b) HP n=1; (c) LP n=1.

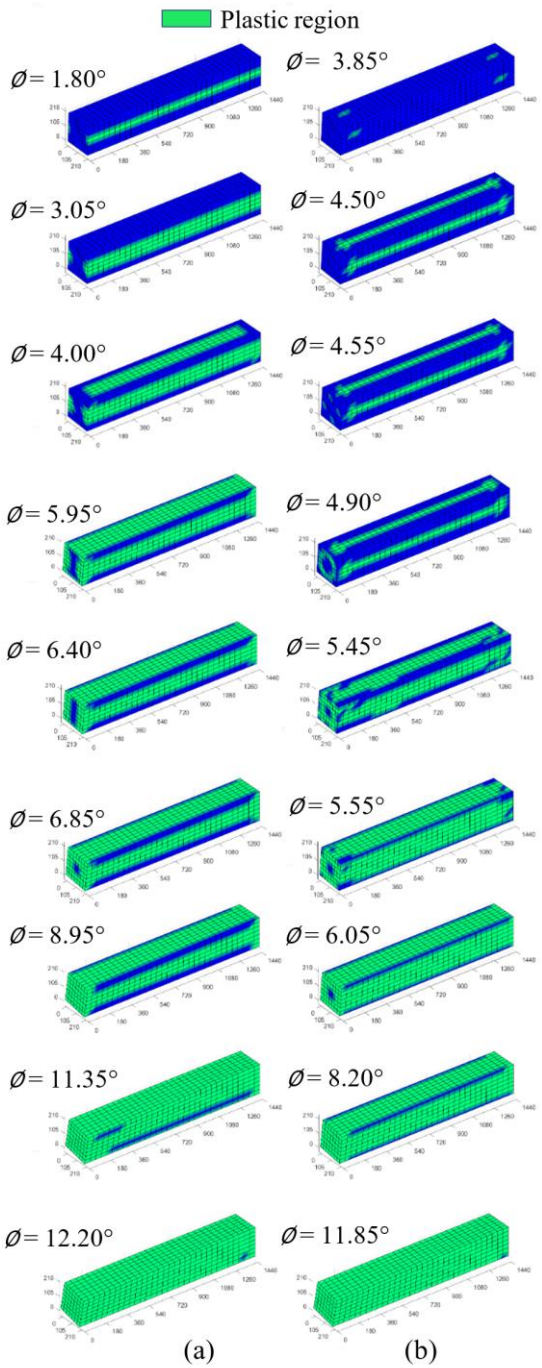

Fig. A2. Distribution of plastic regions in FG beams (a) HS; (b) HBS.